Landslides (2016) 13:925–938
DOI 10.1007/s10346-015-0645-7
Received: 20 March 2015
Accepted: 7 October 2015
Published online: 19 October 2015
© Springer-Verlag Berlin Heidelberg 2015

C. W. W. Ng · V. Kamchoom · A. K. Leung

Centrifuge modelling of the effects of root geometry on transpiration-induced suction and stability of vegetated slopes

Abstract Shallow landslides (i.e. 1–2-m depth) on both man-made and natural slopes are of major concern worldwide that has led to huge amount of socio-economical losses. The use of vegetation has been considered as an environmentally friendly means of stabilising slopes. Existing studies have focused on the use of plant roots with different geometries to mechanically stabilise soil slopes, but there are little data available on the contribution of transpiration-induced suction to slope stability. This study was designed to quantify both the hydrological and mechanical effects of root geometry on the stability of shallow slopes. Centrifuge tests were conducted to measure soil suction in slope models supported by newly developed artificial roots. These artificial roots exhibit three different representative geometries (i.e. tap, heart and plate) and could simulate the effects of transpiration. The measured suction was then back-analysed through a series of finite element seepage-stability analyses to determine the factor of safety (FOS). It is revealed that after a rainfall event with a return period of 1000 years, the slope supported by heart-shaped roots retained the highest suction within the root depth, and thus, this type of root provided the greatest stabilisation effects. The FOS of the slope supported by the heart-shaped roots, through both mechanical reinforcement and transpiration-induced suction, is 16 and 28 % higher than that supported by the tap- and plate-shaped roots, respectively.

Keywords Centrifuge modelling · Plant transpiration · Root geometry · Slope stability · Suction

Introduction

Slope bioengineering using plant roots is an environmentally friendly solution to mitigate rainfall-induced instability of shallow soil slope (i.e. 1–2-m depth). In the past decades, many studies have been carried out to quantify the mechanical effects of root reinforcement through predominantly direct shear and pull-out tests (Fan and Chen 2010; Ghestem et al. 2014; Docker and Hubble 2008). The contribution of real roots to slope stability has also been investigated employing the centrifuge modelling technique (Sonnenberg et al. 2010). Centrifuge model test enables small-scale physical slope models to be tested at the stress levels identical to those experienced by much larger prototypes and under much better controlled test conditions than is possible in field experiments. This technique has been commonly used to study slope stability problems (Take et al. 2004; Wang and Zhang 2014). Although most studies have concluded that the presence of roots can, in general, improve slope stability, it is unclear if roots with certain geometries offer better reinforcement than roots with other geometries. Some research groups have attempted to idealise real root geometries and created artificial roots for assessing pull-out resistance (Stokes et al. 1996; Mickovski et al. 2007; Kamchoom et al. 2014) and quantifying the roots' contribution to mechanical slope stabilisation in centrifuge (Sonnenberg et al. 2012). Most of these studies have, however, generally ignored the hydrological effects of transpiration and the associated-induced soil suction. Laboratory and field tests (Lim et al. 1996; Simon and Collison 2002; Leung and Ng 2013a, b; Ng et al. 2013, among others) have shown that vegetated soil could retain credible suction of up to 20 kPa within root zone for rainfall with return periods less than 10 years. The retained suction could increase shear strength and pull-out resistance of roots (Kamchoom et al. 2014) and also reduce soil hydraulic conductivity (Ng and Leung 2012). Therefore, an improved understanding of the hydrological role of plant transpiration in slope stability is desired.

The objective of this study was to quantify and compare, through centrifuge model tests, the effects of root geometry on slope stability with dual consideration of the hydrological effects of transpiration on suction and the mechanical effects of reinforcement. New artificial roots with three representative geometries—tap, heart and plate—were developed. These roots could simulate both the mechanical properties and hydrological effects of prototype roots observed in the field. To assist the interpretation of test results, a series of finite element seepage-stability analyses were conducted to (i) back-analyse the observed pore water pressure (PWP) responses during transpiration and during rainfall, (ii) evaluate slope stability by determining the factor of safety (FOS) and (iii) quantify the relative contribution of the hydrological and mechanical effects to the FOS against rainfall.

Development of new artificial roots for physical modelling

Idealisation and simplification of root geometry

In order to model both the mechanical and hydrological effects of plant roots with different representative geometries in centrifuge, new artificial roots were developed in this study. In the literature, plant roots can be idealised and categorised as having three typical shapes (Köstler et al. 1968; Stokes and Mattheck 1996), namely tap, heart and plate. Figure 1 shows some real roots retrieved from three species—*Schefflera heptaphylla*, *Rhodomyrtus tomentosa* and *Melastoma sanguineum*—which are commonly used for slope rehabilitation and ecological restoration in tropical and subtropical regions (Hau and Corlett 2003). It can be seen in Fig. 1a that the tap-shaped root consists of one primary root and several secondary roots near its tip. Such root geometry is commonly found in larch species (Stokes and Mattheck 1996). The heart-shaped root shown in Fig. 1b is typical of pine species (Perry 1989). It also has a primary taproot, and its secondary roots are normally found near the soil surface and are predominantly sub-horizontal. As for the plate-shaped root (Fig. 1c) which is common for spruce species (Coutts 1986), it mainly consists of secondary roots spreading out laterally and sub-horizontally at shallow depths. Field observation

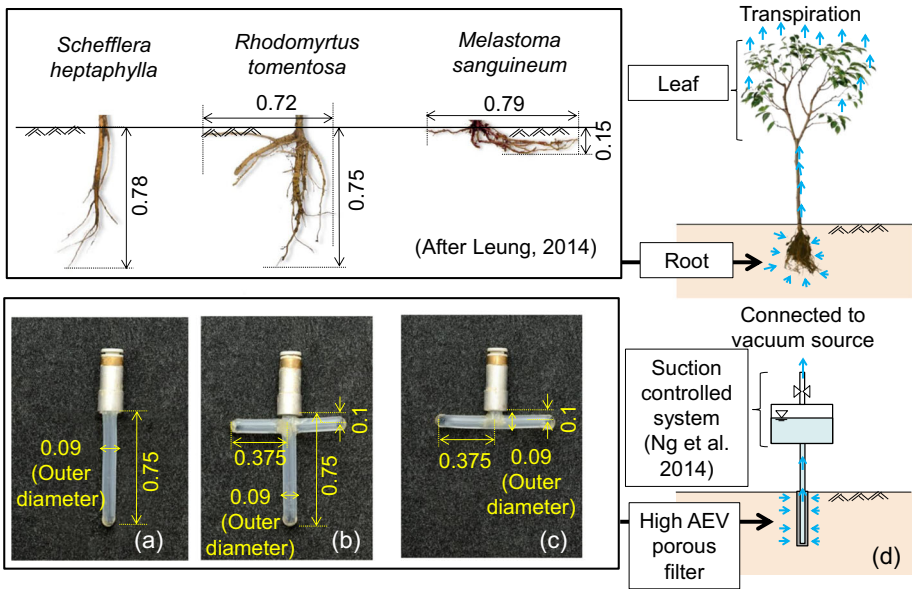

Fig. 1 Overview of **a** tap-, **b** heart- and **c** plate-shaped artificial roots and **d** the newly developed suction-controlled system for simulating the effects of transpiration (Ng et al. 2014) (all dimensions are in meters and in prototype scale)

from Coutts et al. (1999) showed that plants found in slopes commonly have their roots spread predominantly in the in-plane direction for maintaining plant stability.

Based on the three idealised root shapes, three simplified artificial roots were constructed accordingly. Their dimensions shown in Fig. 1 are all expressed in prototype scale, with a scaling factor N of 15, as all centrifuge tests reported in this study were conducted at 15 times gravity (15g). In order to validate these artificial roots, Fig. 2 compares the distribution of root area ratio (RAR; defined as the ratio of cross-sectional area of roots to the soil at a given depth) between artificial and some real roots. For a fair comparison, real roots with each of the three geometries were selected from countries situated in subtropical regions with similar climatic conditions (Table 1). It can be seen in Fig. 2 that for each geometry, reasonably good agreement is found between the real and artificial roots. The observed discrepancies in each case are considered acceptable, given the variability of plants in the field and the idealisation and simplification made for the artificial roots.

Mechanical properties of artificial roots

The material chosen to make the artificial roots was cellulose acetate (CA), as its mechanical and hydraulic properties are suitable for simulating root reinforcement and transpiration-induced suction simultaneously. According to the tensile tests conducted by Ng et al. (2014), CA has an elastic modulus (E) of 83 MPa and a tensile strength (σ_t) of 31 MPa. These mechanical properties of an artificial root are found to be reasonably close to those typically identified in real roots (Coppin and Richards 1990; Stokes and Mattheck 1996). Based on the results of direct shear tests reported by Kamchoom et al. (2014), both the peak and ultimate interface friction angles between the artificial root and the soil to be used in this study are determined to be 34°, which is slightly below the typical range (36.1–37.9°) for soil-real root interface (Wang et al. 2010). For N equal to 15, the prototype axial rigidity (EA, where A is the cross-sectional area of the artificial root) and flexural rigidity (EI, where I is the second moment of inertia of the artificial root) are about 290 kPa m^2 and 0.2 kPa m^4, respectively. This is considerably close to that of a willow (*Salix*) species, which has an E of about 100 MPa at 60-mm root diameter (Stokes and Mattheck

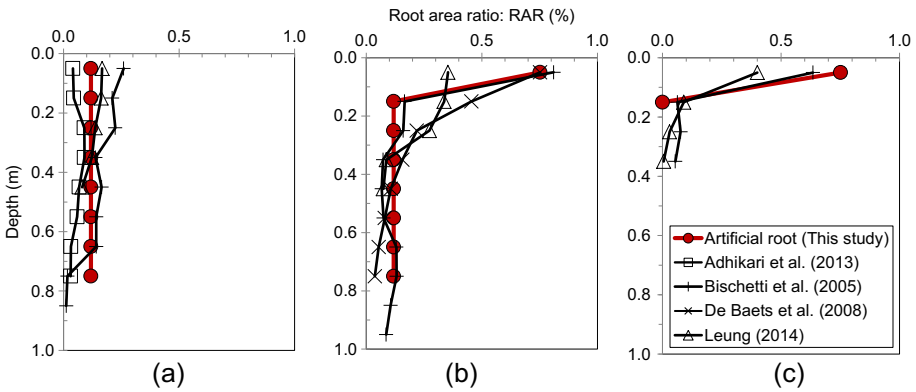

Fig. 2 Comparison between the RAR profiles of **a** tap-, **b** heart- and **c** plate-shaped artificial roots in prototype scale and those of some real roots observed in the field

Table 1 A summary of site characteristics for root area ratio (RAR) comparison in Fig. 2

Case history	Location	Site characteristics				
		Soil type	Climate	Temperature (°C)	Humidity (%)	Slope angle (°)
Adhikari et al. (2013)	Nevada, USA	Sandy soil	Subtropical climate	27–33	20–35	NA
Bischetti et al. (2005)	Northern Italy	Sandy soil	Humid subtropical climate	6–28	60–90	30
De Baets et al. (2008)	Southeast Spain	Colluvium		17–30	60–80	30
Leung (2014)	Hong Kong	Silty sand		16–32	70–90	36

1996). Table 2 summarises all the relevant scaling laws and root properties, both in model and prototype scales.

Simulation of the effects of plant transpiration

In order to simulate the effects of plant transpiration in centrifuge, each artificial root was connected to the suction-controlled system (Fig. 1d) newly developed by Ng et al. (2014). The main idea of the system is to idealise the physical processes of plant root-water uptake and transpiration pull. The system consists of a high air-entry value (AEV), water-saturated porous filter, which is connected to an airtight chamber for applying a vacuum pressure to each root. The applied vacuum would reduce water pressure inside the artificial root, creating a hydraulic gradient to remove the moisture of the surrounding soil. This water flow hence induces soil suction, simulating the effects of plant root-water uptake. This modelling technique has proven to create a range of suction that was typically observed in the field reasonably well (Ng et al. 2014). Besides being a suitable material for modelling the mechanical properties of real roots, CA is also an appropriate porous filter material for simulating the effects of transpiration.

Table 2 A summary of scaling factors relevant to this study

Physical quantity	Dimension	Scaling factor (model/prototype)	Model scale	Prototype scale[a]
Geometry of artificial root				
Length	L	$1/N$	50 mm	750 mm
Outer diameter	L	$1/N$	6 mm	90 mm
Inner diameter	L	$1/N$	4 mm	60 mm
Cross-section area (A)	L^2	$1/N^2$	1.6×10^{-5} m^2	3.5×10^{-3} m^2
Second moment of inertia (I)	L^4	$1/N^4$	5.1×10^{-11} m^4	2.6×10^{-6} m^4
Material property of artificial root				
Tensile strength of artificial root (σ_t)	M/LT^{2b}	1	3.1×10^4 kPa	3.1×10^4 kPa
Elastic modulus of artificial root (E)	M/LT^2	1	8.3×10^4 kPa	8.3×10^4 kPa
Axial rigidity (EA) of taproot component	ML/T^2	$1/N^2$	1.3 kPa^{a}m^2	2.9×10^2 kPa^{a}m^2
Flexural rigidity (EI) of horizontal root branch	ML^3/T^2	$1/N^4$	4.2×10^{-6} kPa^{a}m^4	2.2×10^{-1} kPa^{a}m^4
Air-entry value of filter	M/LT^2	1	100 kPa	100 kPa
Hydraulic conductivity of filter	$L/T_{diff}{}^b$	N	2×10^{-6} m/s	1.3×10^{-7} m/s
Soil-atmosphere interface				
Rainfall intensity[c]	L/T_{diff}	N	1050 mm/h	70 mm/h
Seepage				
Water flow rate[b]	$L^3/T_{diff}{}^b$	$1/N$	Depend on measurements	
Hydraulic conductivity[b]	$L/T_{diff}{}^b$	N		
Hydraulic gradient[b]	Unitless	1		
Suction[d]	M/LT^2	1		

[a] Prototype scale at g-level of 15 (i.e. N=15)

[b] Time for dynamic condition (T) is scaled by $1/N$, whereas time for diffusion (T_{diff}) is scaled $1/N^2$

[c] According to Taylor (1995)

[d] According to Dell'Avanzi et al. (2004)

Table 3 A summary of soil and root properties and the input parameters used for the finite element seepage-stability analyses

	Parameter	Value	Unit	Reference
Soil index properties	Bulk unit weight (γ_t)	20	kN/m^3	Ho (2007)
	Specific gravity (G_s)	2.59	–	
	Maximum dry density	1890	kg/m^3	Standard Proctor compaction tests (BSI 1990)
	Optimum moisture content	15.1	%	
	Sand content (≤2 mm)	56.8		Laboratory tests
	Silt content (≤63 μm)	39.1		
	Clay content (≤2 μm)	4.1		
	D_{10}	0.005	mm	
	D_{30}	0.041		
	D_{50}	0.081		
	D_{60}	0.115		
	Plastic limit (PL)	22.7	%	
	Liquid limit (LL)	32.8		
	Plasticity index (PI)	10.1		
Mechanical properties of soil	Effective cohesion (c')	0	kPa	Hossain and Yin (2010)
	Critical state friction angle (φ_{cr}')	37.4	°	
	Dilation angle (ψ)	5	°	
	Young's modulus (E)	35	MPa	Zhou (2008)
	Poisson's ratio (v)	0.26	–	
Hydraulic properties of soil	Saturated hydraulic conductivity (k_s)	1×10^{-7}	m/s	Falling head tests
	Air-entry value (AEV)	1	kPa	Ho (2007)
	Saturated water content (Θ_s)	See Fig. 3	%	SWRC measured by Ho (2007) and then fitted by van Genuchten (1980)
	Residual water content (Θ_r)			
	Fitting parameters for van Genuchten (1980) α		kPa^{-1}	
	Fitting parameters for van Genuchten (1980) n		–	
	Fitting parameters for van Genuchten (1980) m			
Mechanical properties of artificial roots	Tensile strength (σ_t)	3.1×10^4	kPa	Root tensile tests (Ng et al. 2014)
	Young's modulus (E)	8.3×10^4	kPa	
	Interface friction angle (δ')	34	°	Direct shear tests (Kamchoom et al. 2014)
Hydraulic properties of artificial roots	Saturated hydraulic conductivity (k_s)	2×10^{-6}	m/s	Ng et al. (2014)
	Air-entry value (AEV)	100	kPa	

This is because the CA has a high AEV of up to 100 kPa for maintaining water pressure produced by any vacuum applied through the chamber. The working principle of the suction-controlled system is explained in more detail in Ng et al. (2014).

Centrifuge modelling and test programme

Test plan

Three centrifuge tests were conducted in total to quantify and compare the contributions of the three different root geometries (tap, heart and plate) to induced suction and the associated stability of 45° slope models. Each slope model supported by multiple artificial roots was subjected to a period of "transpiration" using the new suction-controlled system followed by a rainfall event. All centrifuge tests were carried out at 15*g* in the geotechnical beam centrifuge facility at the Hong Kong University of Science and Technology. The fundamental principle of centrifuge modelling is to recreate stress conditions, which would exist in a prototype. Stress replication in the 1/N scaled model is approximately achieved by subjecting model components to *N* times of a "gravitational" acceleration, which is provided by centripetal acceleration (Taylor 1995; Ng 2014).

Soil type and properties

Each slope model tested in this study was made of re-compacted completely decomposed granite (CDG) taken from Beacon Hill,

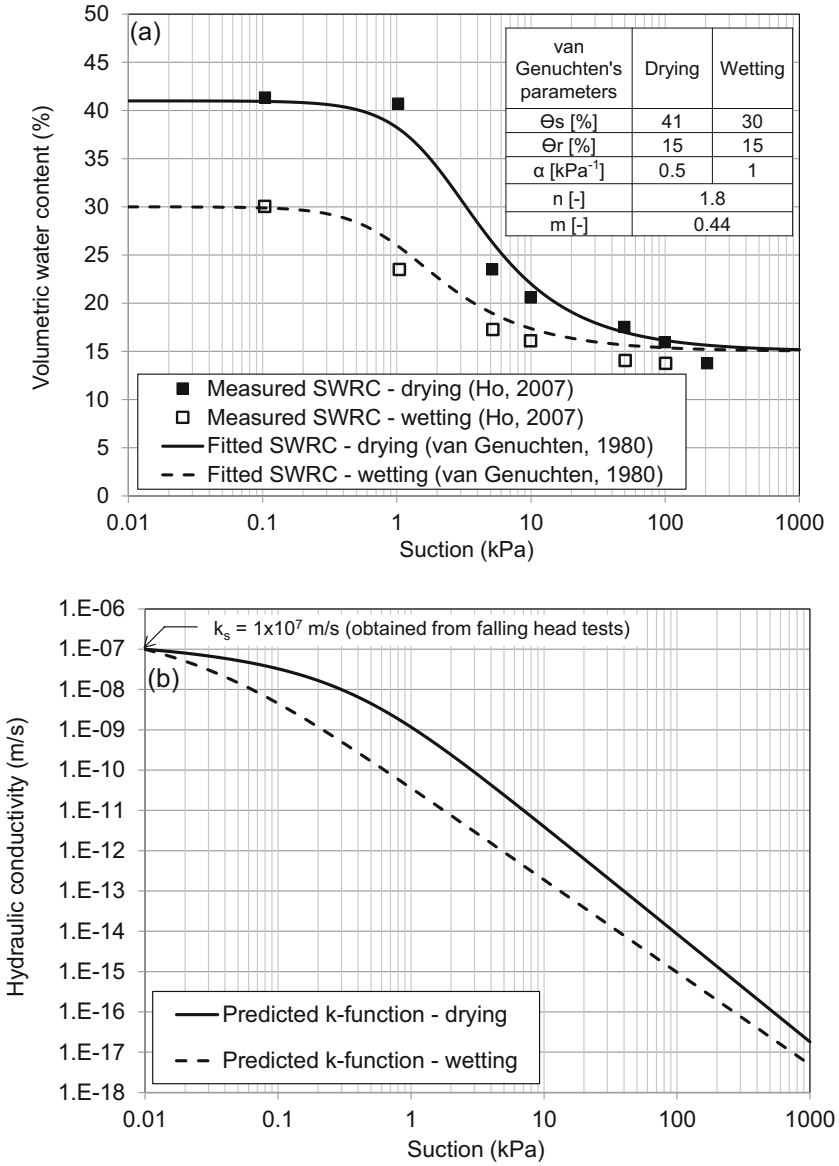

Fig. 3 **a** Measured and fitted soil water retention curves (SWRC) and **b** predicted hydraulic conductivity function of CDG. *k* indicates hydraulic conductivity, and k_s is saturated hydraulic conductivity

Hong Kong. In order to minimise any particle size effects in centrifuge tests (Taylor 1995), CDG with particle sizes larger than 2 mm was sieved. As a result, the ratio between the diameter of artificial roots (D_r) and D_{50} of the soil (i.e. D_r/D_{50}) was 74. This ratio was well above the critical ratio of 30, which was identified to be the upper limit that the particle size effects might become insignificant (Ovesen 1979; Bolton et al. 1993). At a dry density of 1777 kg/m^3 (i.e. equivalent to a relative compaction of 95 %), the re-compacted CDG has zero effective cohesion (c'), an effective critical state angle (ϕ_{cr}') of 37.4° and a dilation angle (ψ) of 5° (Hossain and Yin 2010). More measured properties of CDG are summarised in Table 3.

A pair of measured drying and wetting soil water retention curves (SWRCs) of CDG using pressure plate apparatus is depicted in Fig. 3a. Each curve was obtained using pressure plate apparatus following the test procedures adopted by Ng and Pang (2000). Each SWRC was fitted with the equation proposed by van Genuchten (1980), and the fitting parameters (α and n) are summarised in the figure. Hydraulic conductivity functions (Fig. 3b) along the drying and wetting paths were estimated using a combination of the prediction equation proposed by van Genuchten (1980) and saturated hydraulic conductivity k_s measured through a series of falling head tests. These hydraulic properties were later used as input for the transient seepage analyses.

Model preparation and instrumentation

In each test, the model package consisted of two major components; (i) a strong box for storing a 45° slope model supported by multiple artificial roots of the same geometry and (ii) a rainfall simulation system for controlling the rainfall intensity and duration. Figure 4 shows the procedures for preparing a model soil slope inside the strong box. Before compacting each model slope,

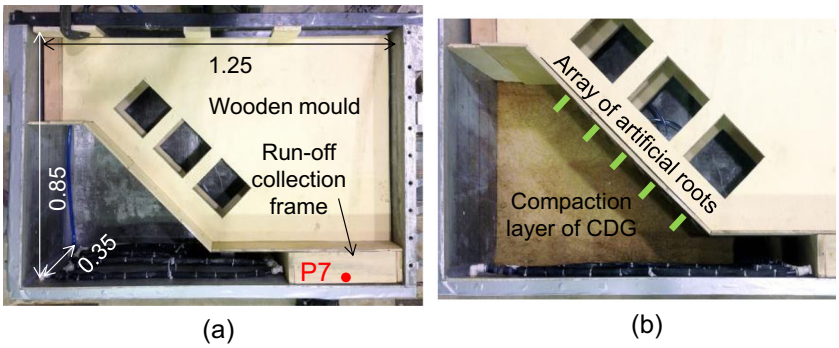

Fig. 4 Images of **a** the mould setup and **b** arrangement and installation of artificial roots during soil compaction (all dimensions are in meters)

silicone grease was pasted on all sides of the strong box. This type of grease is commonly used to minimise any undesirable friction and preferential flow of rainwater between the interface of the soil and all the boundaries of the strong box (i.e. Powrie 1986; McNamara and Taylor 2004). As shown in Fig. 4a, a wooden mould identical in shape to the slope model was fitted inside the strong box. The face of the mould covering the slope surface had holes drilled into it. This facilitated the installation of artificial roots later on (Fig. 4b). A total of 15 artificial roots were arranged in three columns × five rows with an identical spacing of 1.73 m. All roots were installed perpendicularly to the slope surface. The spacing of 1.73 m was selected so that the RAR would be consistent with the field observation shown in Fig. 2. The strong box was then laid down, and the CDG at gravimetric water content of 15.1 % was compacted to a dry density of 1777 kg/m^3 in six layers using undercompaction method (Ladd 1977). After compacting each of the first, third and fifth layers, an array of five artificial roots were inserted through the pre-drilled holes. Each artificial root was connected to the suction-controlled system through a rubber tube and vacuum delivery panel (Fig. 5). The rubber tubes were sufficiently long so as to allow the roots' free movement as the slope deformed during testing inflight. After the installation of all the artificial roots and soil compaction, the wooden mould was removed. A lid was then placed over the strong box to minimise any evaporation from the bare soil surface, as well as any soil suction change due to the strong wind created by centrifuge spinning. The bottom and side boundaries of the strong box were set to be impermeable, and no water table was controlled in all tests. The slope surface was left exposed for rainfall infiltration. The rainfall simulation system consisted of six nozzles mounted inside the strong box (Fig. 5a) and could produce mist droplets as rainfall. The use of mist droplets to simulate rainfall has the advantage of reducing the impact energy that might cause soil erosion and of mitigating droplet deviation (Caicedo and Tristancho 2010).

Four pore-pressure transducers (PPTs; Druck PDCR-81), namely P1 to P4, were installed in each slope model to monitor the responses of PWP at the mid-slope (Fig. 5). Two PPTs (P5 and P6) were installed at the bottom part of each model slope to monitor any development of groundwater table (GWT) during testing. Each PPT consisted of a saturated 1-bar AEV ceramic filter for measuring negative PWPs. Prior to installation, a cylindrical rod with a diameter slightly smaller than that of a PPT was drilled horizontally from the back of strong box into the location of each PPT (Fig. 5a). Since the scaling factor of suction was identified to be 1.0 (Dell'Avanzi et al. 2004; Table 2), any suction recorded in the model box at 15*g* was equal to that in prototype.

During a rainfall event, any surface runoff generated from the slope models was measured by a runoff collection frame (340 mm in

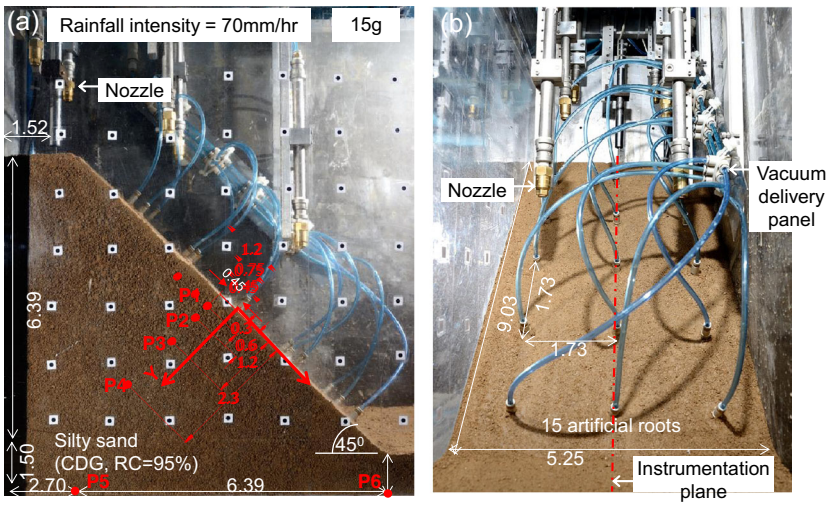

Fig. 5 **a** Elevation and **b** side views of the centrifuge model package and instrumentation (all dimensions are in meters and in prototype scale)

length×340 mm in width×100 mm in height) attached to the strong box near the slope toe (see Fig. 4a). Another PPT, namely P7, was mounted inside the frame for monitoring any build-up of water pressure due to the accumulation of surface runoff water. As a result, the infiltration rate in the slope models can be determined by the difference between applied rainfall intensity and measured runoff.

Test procedures

Each centrifuge test was carried out in five stages. In the first stage, the centrifuge model package was spun up in the centrifuge (waypoint A), until the centrifugal acceleration reached 15*g* (i.e. waypoint B). The second stage was to maintain the 15*g* acceleration for the soil mass to consolidate so as to dissipate any excess PWP that might have built up as the g-level rose in the first stage. The 15*g* consolidation of the soil mass was considered to be completed when all PPTs showed negligible change in PWP (waypoint C). In the third stage at waypoint C, the effects of transpiration were simulated by applying an identical vacuum pressure to all artificial roots through the suction-controlled system. The vacuum pressure was kept constant, again until all PPTs showed negligible change in PWP within 24 h in prototype (waypoint D). Subsequently, in the fourth stage, a rainfall event was applied through the nozzles, with a constant intensity of 70 mm/h for 36 h. According to Lam and Leung's (1995) statistical analysis of 100 years' rainfall data in Hong Kong, the return periods for rainfall lasting 2 and 8 h (waypoint E) are 10 and 1000 years, respectively. Rainfall was terminated at waypoint F and the test drew to an end at waypoint G. After spinning down, it was observed that all three slope models remained standing. Stability analysis was conducted later to support this observation.

Numerical modelling of transient seepage and stability of root-supported slopes

In this study, a series of six finite element seepage-stability analyses was performed. The first three analyses aimed to back-analyse the PWP responses induced by the artificial roots and determine the FOS of the three rooted slopes tested in the centrifuge. Transient analyses were carried out first using SEEP/W (Geo-Slope Int. 2009a; based on mass balance equation and Darcy's law) to simulate the seepage event from waypoints C to D (i.e. the simulation of transpiration) and also from waypoints D to E (i.e. the simulation of rainfall). Then, slope stability analyses were conducted using the finite element program SIGMA/W (Geo-Slope Int. 2009b) to determine FOS through strength reduction method (SRM; Dawson et al. 1999; Griffiths and Lane 1999; Ng et al. 2001) at waypoints C, D and E. The other three analyses repeated the first three, but without considering the effects of transpiration. These analyses would provide insights into the significance of transpiration for slope stability.

Figure 6 shows a typical finite element model adopted for the case of heart-shaped roots, analysed in prototype scale. For each seepage analysis (Fig. 6a), the hydraulic boundary conditions of each slope were set identical to those in the centrifuge tests. To model three-dimensional (3D) artificial roots in a two-dimensional (2D) plane-strain slope model, a similar equivalent approach proposed by Indraratna and Redana (1997) was adopted. Each artificial root was modelled by creating a hollow material for each root component (i.e. tap part and branches) and then connecting them together. As all artificial roots were made of CA, AEV of 100 kPa and a saturated hydraulic conductivity of 1×10^{-6} m/s were specified to all the components. The internal width of each root component was adjusted so that the total capacity of water volume flow in this 2D plane-strain "root wall" is equal to that in the 3D circular root tested in the centrifuge. The thickness of each root component was maintained to be the same as those tested in the centrifuge (i.e. 15 mm in prototype type; Fig. 1). A constant pressure head was then applied along the internal boundary of each root component to simulate the effects of transpiration. Although a constant vacuum pressure of 95 kPa was applied in all the experiments, the pressure head applied in each root was corrected by the elevation head difference between each artificial root and the water level maintained in the vacuum chamber (i.e. at the same elevation of the slope crest).

The first three transient seepage analyses consisted of three stages. The first stage was to specify a GWT that could produce a PWP distribution similar to those recorded by all the PPTs at waypoint C right before the simulation of transpiration. In the second stage, the vacuum pressure applied in each artificial root in the centrifuge tests was simulated (i.e. from waypoints C to D). In this stage, the set of soil drying parameters presented in Fig. 3 were used. When waypoint D was reached, the third stage of analysis began. The infiltration rate measured in the centrifuge was applied at the slope surface for simulating the 8-h rainfall event (i.e. from waypoints D to E). In an attempt to consider the effects of hysteresis identified in Fig. 3, the set of soil wetting parameters were used in this stage. For the other three analyses (where transpiration was not considered), only the first and third stages were performed.

For the calculation of slope stability using SIGMA/W, the identical slope geometry and finite element mesh from SEEP/W were adopted. The side boundary of the slope was set to allow for vertical movement, while a fixed boundary was assigned at the bottom of slope to restrict both the vertical and horizontal movements. The CDG was modelled as a perfectly plastic material that obeys the modified extended Mohr-Coulomb failure criterion (Vanapalli et al. 1996):

$$\tau_s = c' + (\sigma_n - u_a)\tan\phi_{cr}' + (u_a - u_w)\left[\left(\frac{\theta_w - \theta_r}{\theta_s - \theta_r}\right)\tan\phi_{cr}'\right] \quad (1)$$

where τ_s is the shear strength of soil (kPa); c' is the effective cohesion (kPa), which is equal to zero for the re-compacted CDG; σ_n is the normal stress on a slip surface (kPa); u_a is the pore-air pressure (considered to be atmospheric, i.e. zero) (kPa); ϕ_{cr} is the critical state friction angle (°), which is equal to 37.4°; u_w is the PWP (kPa) and θ_w is the volumetric water content (VWC) ($m^3\ m^{-3}$); θ_s is the VWC at saturation ($m^3\ m^{-3}$); and θ_r is the VWC at residual state ($m^3\ m^{-3}$). All input parameters are summarised in Table 3. To model the mechanical properties of each root component, a beam element (Hinton and Owen 1979) was used to capture both the elastic axial and bending responses by specifying the Young's modulus, cross-sectional area and the moment of inertia of each root component (see Table 3). The soil-root interface was simulated using an interface element, allowing for soil-root interaction such as axial and bending strength mobilisation to be considered. The interface element also follows Mohr-Coulomb failure criterion, and the interface friction angle was specified as 34° (Kamchoom et al. 2014). A similar modelling approach was used to capture the interface behaviour between soil and structures, such as nails (i.e. Yang and Drumm 2000; Kim et al. 2013).

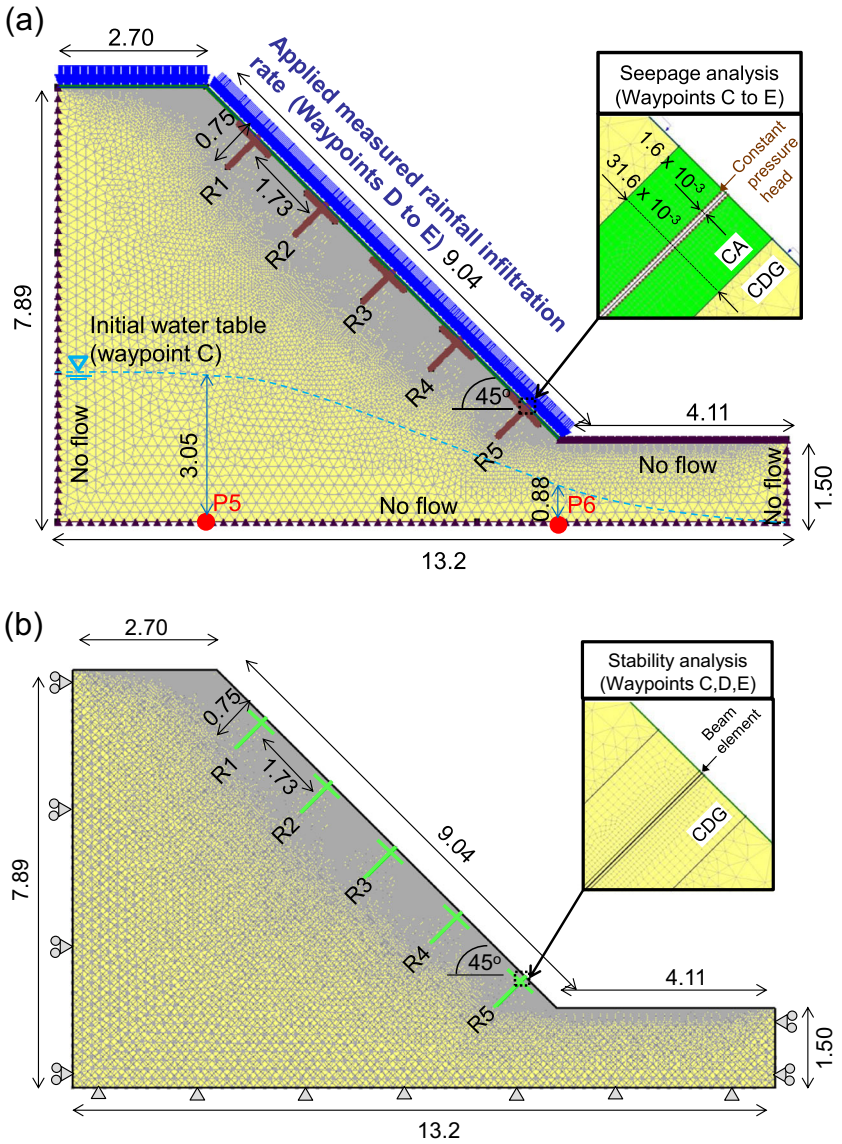

Fig. 6 A typical finite element mesh of the slope supported by heart-shaped roots for **a** seepage and **b** stability analyses (all dimensions are in meters and in prototype scale)

When modelling the heart- and plate-shaped roots, the connection between the taproot and their branches was assumed to be rigid. In each stability analysis, the PWP distributions computed at waypoints C, D and E from SEEP/W were inputted into SIGMA/W for determining FOS using SRM. The principle of SRM is to apply a factor that would continuously reduce the shear strength parameters (i.e. c' and ϕ_{cr}') until the slope could not maintain its equilibrium. During the shear strength reduction, imbalanced force would be developed in the slope. The roots installed in the slope would interact with the surrounding soil and mobilise any of their axial and bending strengths in resisting the loss of stability of each slope. The strength reduction factor that arrives at the non-equilibrium condition of the slope is referred to as FOS. Compared to limit equilibrium method, the SRM eliminates the need to pre-define any search algorithm and any prior assumptions on the shape and location of a failure surface.

Interpretation of measured and computed results

Variations in PWP against time

Figure 7a–c shows the measured PWP variations with time of slopes containing tap-, heart- and plate-shaped roots, respectively. Note that the response recorded by P4 in the slope model supported by tap-shaped roots is not shown because, unfortunately, this particular PPT was desaturated during the test. Prior to centrifuging, the initial PWP recorded by all PPTs was about −15 kPa for all three slope models. As the g-level rose, PWP jumped at all instrument locations in all three slope models due to self-weight consolidation. Similar PWP responses were also reported by Take et al. (2004) for an unsaturated CDG slope. When 15*g* was reached at waypoint B, the PWP reduced, but at rates much lower than the increases observed during the rise of g-level. This was likely attributed to the dissipation of the excess PWP generated in the previous stage. When vacuum pressure of

−95 kPa was applied to simulate the effects of transpiration (waypoint C), PWP reduced substantially at depths of 0.3 and 0.6 m in the slopes supported by the tap- and heat-shaped roots (Fig. 7a, b). On the contrary, for the slope supported by the shallower plate-shaped roots (Fig. 7c), only PWP at a depth of 0.3 m showed some reduction. This goes to show that the root geometry played a significant role in affecting the distribution of induced suction. When PWP equilibrium was reached after the application of vacuum (waypoint D), rainfall was applied. Upon infiltration, the PPTs in the top 1.2 m of soil in all three slopes were found to show significant increases in PWP to around −1 and −2 kPa and further to a positive value of about 10 kPa at a depth of 2.3 m after 8 h of rainfall (at waypoint E). As the rainfall event continued (i.e. waypoints E to F), the measured increases in PWP were less significant, and they appeared to reach the steady state.

Effects of root geometry on induced suction during drying

Figure 8a compares PWP responses measured along depth among the three slopes. At 15*g* (i.e. waypoint C), the measured PWP profiles in all three slopes were very similar to each other. When the vacuum pressure of −95 kPa was applied, the measured PWP within the root depth of the tap-shaped root (Fig. 8a) decreased substantially from a value of about −20 to −26 kPa. On the contrary, PWP below the root depth of 1.2 m showed only a slight decrease of about 2 kPa. For the slope supported by heart-shaped roots (Fig. 8b), PWP at a depth of 0.3 m is found to be 15 % higher in that slope than in the one supported by tap-shaped roots (Fig. 8a). This is because the heart-shaped root has two additional root branches (see Fig. 1b) which served to induce a greater reduction in PWP. However, since the two branches were located at a relatively shallow depth of 0.1 m, their depth of influence on PWP appeared to be up to 0.3 m. This explains why the PWP induced at a depth of 0.6 m was similar between the two cases (i.e. about −26 kPa). For the slope supported by plate-shaped roots (Fig. 8c), it appears that induced PWP was affected mainly at the shallow depths around the two branches (i.e. at 0.3 m), whereas those at greater depths than this were much less significant.

It can be seen that the computed PWP profiles agree well with the measurements made in all three cases, both before and after rainfall. It is therefore safe to say that the simulation of the transpiration effects in the centrifuge was fairly accurately back-analysed when a constant head of −9.5 m was applied along the

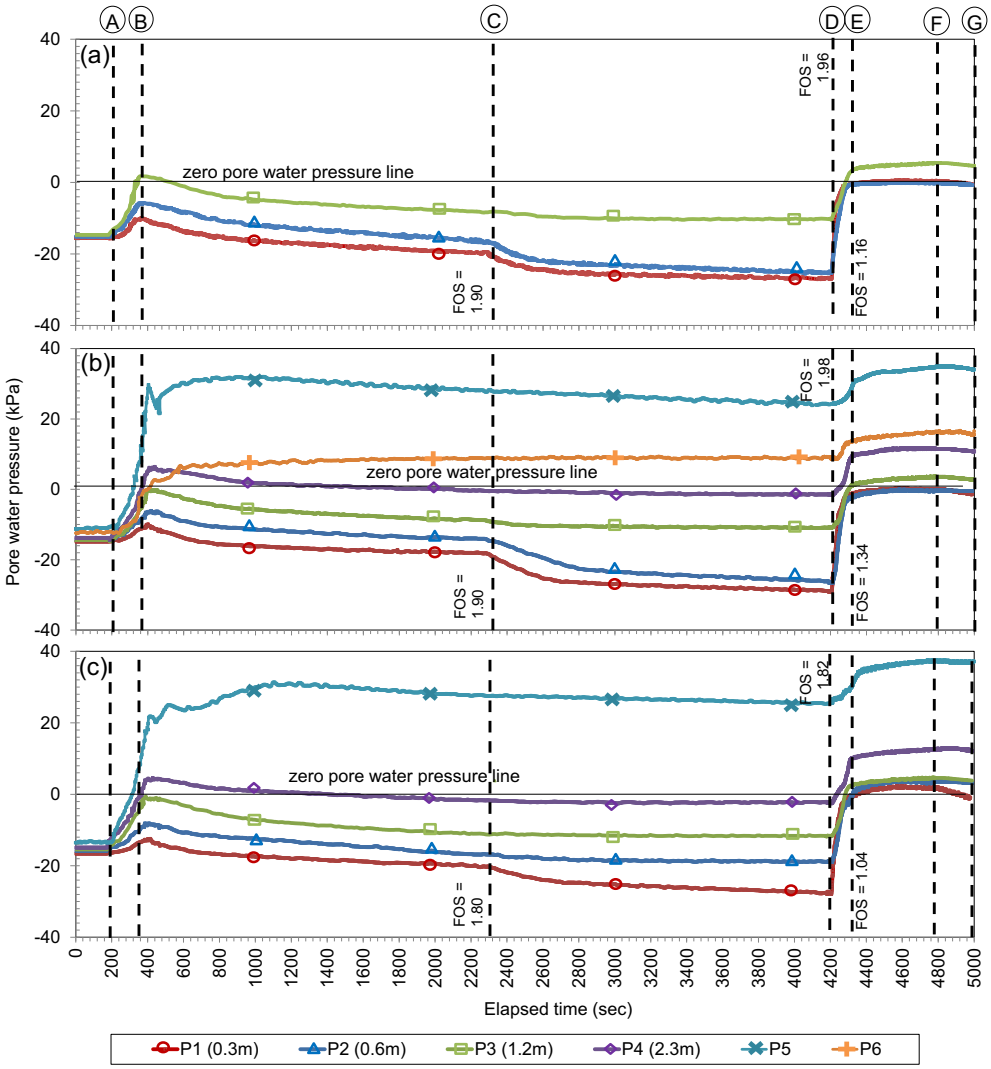

Fig. 7 Measured variations in pore water pressure with time for slope models supported by **a** tap-, **b** heart- and **c** plate-shaped roots

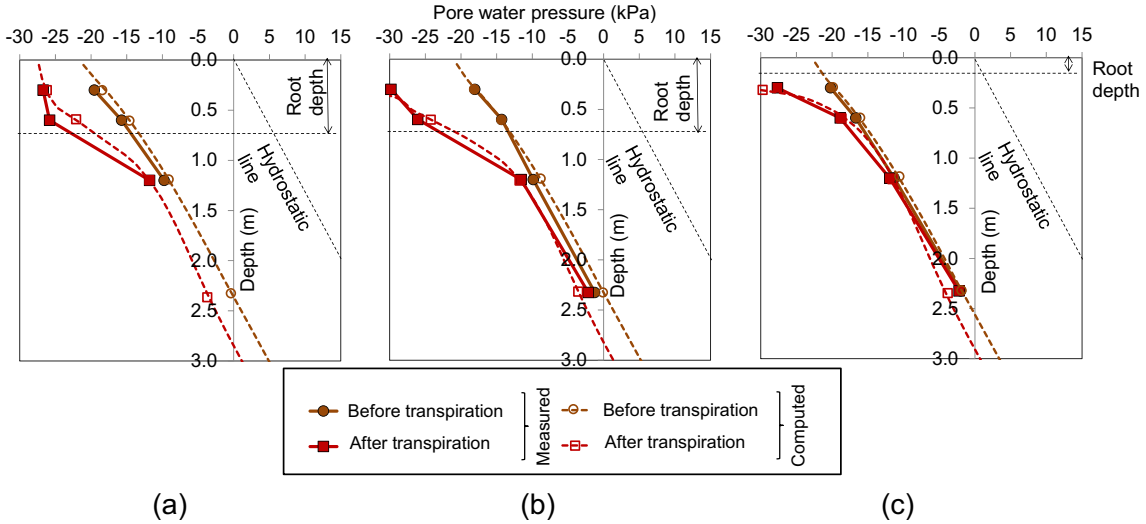

Fig. 8 Distribution of measured and computed pore water pressure along depth before (waypoint C) and after "transpiration" (waypoint D) for slope models supported by **a** tap-, **b** heart- and **c** plate-shaped roots

root boundaries. The close agreement between the measurements and the simulations also suggests that the seepage modelling provided reasonable PWP responses that can be reliably used for the subsequent stability analyses.

Effects of root geometry on water infiltration and suction during rainfall

Figure 9 compares the measured variations in the water infiltration rate with time among the three slopes. As the rainfall was maintained at a constant intensity of 70 mm/h, the initial infiltration rates in the first hour remained constant in all three slopes. However, when infiltration capacity was reached, all measured rates reduced exponentially, approaching the k_s of the CDG. The infiltration rate in the slope supported by the heart-shaped roots was lower than that in the slope supported by the tap-shaped roots, while the one supported by the plate-shaped roots had the highest infiltration rate. The observed trend is consistent with the measured PWP responses. As shown in Fig. 8, the PWP induced in the case of heart-shaped roots at the shallowest measurement depth of 0.3 m was the lowest, which would have caused the greatest reduction in hydraulic conductivity among the three cases (Fig. 3b). Although similar amounts of PWP were induced in the cases of tap- and plate-shaped roots (Fig. 8), the PWP induced at a depth of 0.6 m by tap-shaped roots was much lower than that induced by plate-shaped roots. This thus led to the noticeable difference between their water infiltration rates in Fig. 9. For the purpose of seepage modelling, each measured infiltration rate was best-fitted. Each fitted line was then imposed on the slope surface boundary in SEEP/W for simulating the wetting event (see Fig. 6).

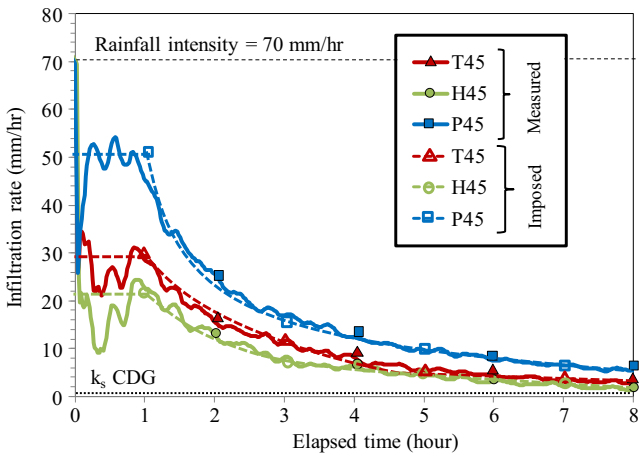

Fig. 9 Measured variations in the infiltration rate with time and the best-fitted lines used for seepage analyses

Figure 10 compares the measured PWP profiles of the three slopes during rainfall infiltration. Note that the initial PWP profiles before rainfall were identical to those after drying in all three cases as presented in Fig. 8. For the slope supported by tap-shaped roots (Fig. 10a), PWP at the shallowest depth of 0.3 m showed the most significant increase after 2 h of rainfall (equivalent to a 10-year return period), whereas the increase was smaller at depths below the root depth. The seepage analysis also gave similar magnitudes of suction at the three instrument depths, although a positive PWP of about 5 kPa was developed within 0.3 m of the slope surface. As rainfall continued for another 6 h (equivalent to a 1000-year return period), PWP at all depths increased further. However, the amount of PWP increase within the root depth was much smaller than that below the root depth. This resulted in some negative PWP of about −2 kPa retained in the shallower depths, while a positive PWP of about 4 kPa was built up at a depth of 1.2 m. This highlights the significance of the effects of transpiration simulated by the artificial roots for suction redistribution. Figure 11a shows the computed PWP contour after 8 h of rainfall for the tap-root case. It can be seen that a zone of negative PWP was retained around the roots, especially for roots located in the upper part of the slope. This suction retained due to the effects of transpiration reduced soil hydraulic conductivity and, hence, the infiltration rate at the later stage of the rainfall event (Fig. 9). Below the root depth where PWP was less influenced by transpiration, the PWP profile exhibited an almost hydrostatic distribution (Fig. 10a) and a GWT was developed (Fig. 11a). The seepage analysis appears to give a fairly good prediction of the PWP recorded in the slope (see also Fig. 7a).

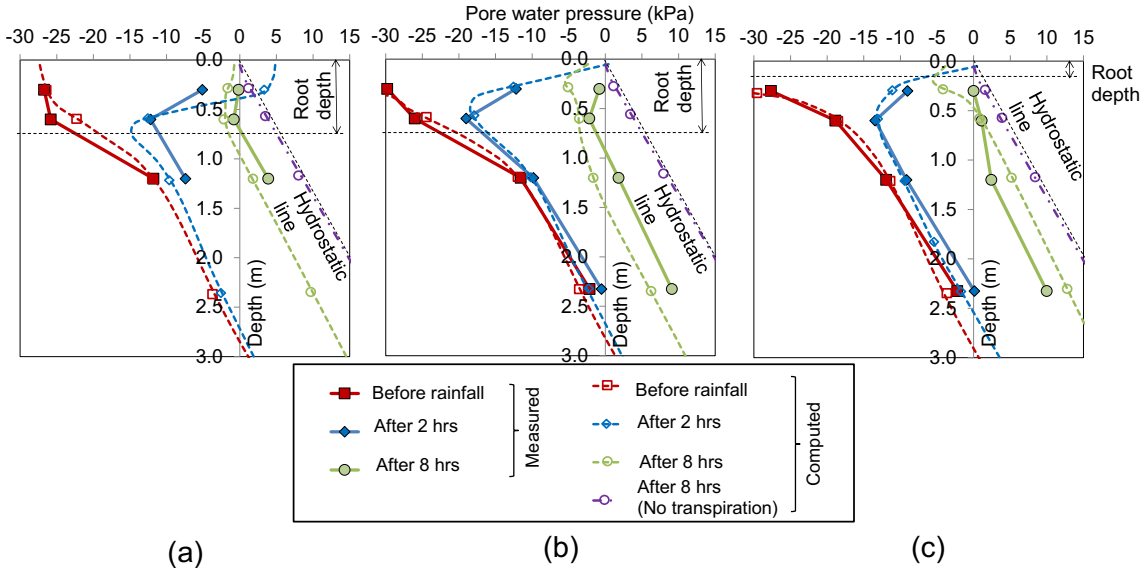

Fig. 10 Distribution of measured and computed pore water pressure along depth before rainfall (waypoint D) and after 2 and 8 h (waypoint E) of rainfall in slope models supported by **a** tap-, **b** heart- and **c** plate-shaped roots

As for the slope supported by heart-shaped roots (Fig. 10b), the measured responses of PWP were largely similar to those observed in the case of tap-shaped roots, even though in the former case, (i) the initial PWP before rainfall was considerably lower (about 15 %) and (ii) the water infiltration rate shown in Fig. 9 was slightly lower. After raining for 8 h, the measurements showed that rather similar suctions of 2–3 kPa were retained within the root depth in the cases of tap- and heart-shaped roots. However, the computed PWP contour depicted in Fig. 11b shows that the zone of negative PWP developed was larger than that found in the tap-rooted case (Fig. 11a). This suggests that the additional root branches of heart-shaped roots have helped extending the influence zone of transpiration to affect the PWP regime of the slope in deeper regions. A similar GWT was found after 8 h of rainfall. The positive PWP built up in the numerical model is found to be consistent with the measurements made by P5 and P6 at the bottom of the slope (see also Fig. 7b).

For the case of plate-shaped roots which have a much shallower root depth (Fig. 10c), the PWP responses measured during the first 2 h of rainfall were again similar to those for the cases of tap- and heart-shaped roots at all instrument depths. However, as rainfall continued, only little suction was retained in the root zone, while positive PWPs were recorded at all depths and distributed hydrostatically. These measured PWP responses are consistent with the computed PWP contour shown in Fig. 11c. The contour shows that mainly localised suction was retained near the roots and the suction zone developed around the roots was smaller than those found in the tap- and heart-root cases. This is mainly because the plated-shaped roots do not have a taproot component, and their induced suction thus has less influences in deeper depths. Although the computed PWP at the end of the rainfall event was slightly underestimated in the top 0.5 m of soil in the plate-root case (Fig. 10c), those at deeper depths were fairly close to the measurements. Given the limitation and simplification made in the seepage analyses, the discrepancies between measured and computed PWP are considered acceptable.

Effects of root geometry and transpiration on slope stability and deformation

Figure 12 compares the FOS of the slopes supported by roots with the three different root geometries at waypoints C (i.e. after consolidation), D (i.e. after 5 days of transpiration) and E (i.e. after 8 h of rainfall). Before transpiration, FOS is found to be similar for all three slopes and it is higher than 1.0 (i.e. stable). Figure 13a–c shows the corresponding mobilisation of shear strain contours in the slope. The initial suction developed in shallow depth, together

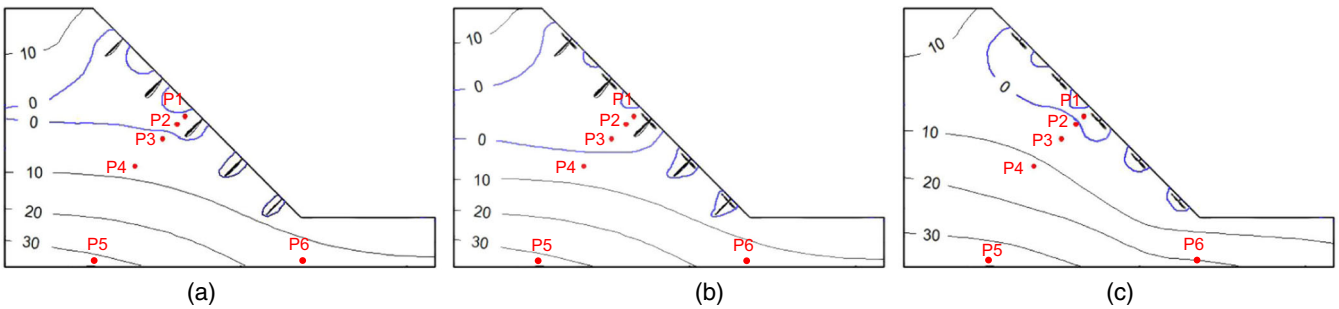

Fig. 11 Computed pore water pressure contour after 8 h of rainfall (waypoint E) in slope models supported by **a** tap-, **b** heart- and **c** plate-shaped roots

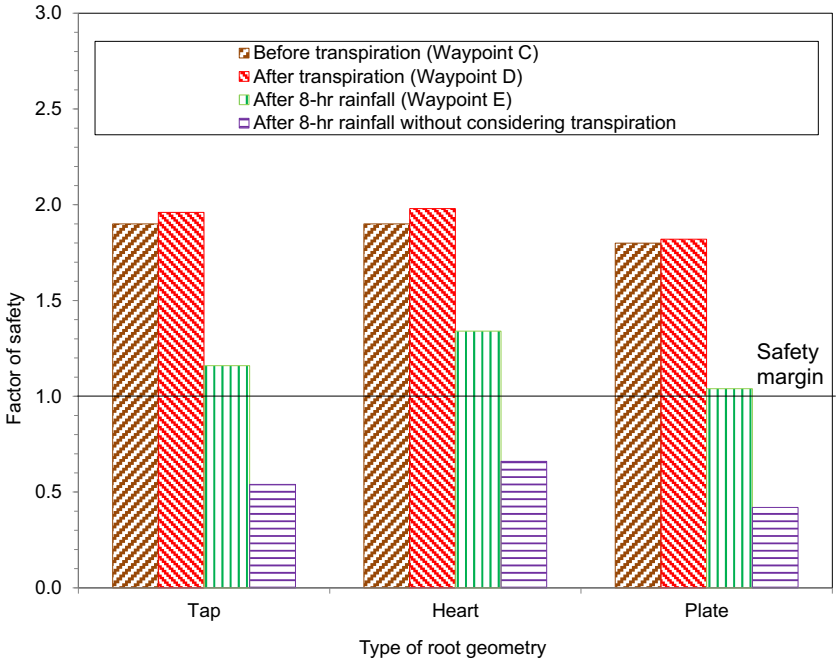

Fig. 12 Computed values of FOS for slopes supported by different root geometries

with the mechanical reinforcement contributed by the artificial roots, created sufficient strength for the shallow soil to maintain its stability. Shear strain thus occurred in deeper depths below the root zone. Localised shear strain of up to 200 % was mobilised, indicating the potential formation of slip plane where the sliding mass above would fail along. As strain mobilisation mainly occurred in depths deeper than the root length, the shallow stability of all slopes (up to 1 m) was adequately maintained by the roots. When suction was created by the artificial roots through the simulation of transpiration (refer to Fig. 8), it can be seen in Fig. 12 that the FOS of each slope increased, though not very significantly (i.e. less than 4 %). When considering the corresponding shear strain contour in Fig. 13d–f, strain localisation apparently occurred at the same position before transpiration. This is because transpiration affected mainly the PWP in the top 1.2 m of each slope (see Fig. 8). This means that induced suction provided an additional stabilisation at the relatively shallow depths (i.e. within 1.2 m of the soil surface).

After raining for 8 h (i.e. waypoint E), the FOS of all three slopes dropped significantly (Fig. 12), following the reduction in PWP upon infiltration. Shear strain appears to have substantially intensified near the toe of each slope after the rainfall (Fig. 13g–i), as compared to the cases before rainfall. Despite of the reduction of the FOS, the values in all three cases are still higher than 1.0, consistent with the centrifuge observation that all slopes remained standstill. The FOS of the slope supported by the heart-shaped roots is found to be 16 and 28 % higher than that supported by the tap- and plate-shaped roots, respectively. The greater stability provided by the heart-shaped roots is mainly because of the substantial amount of suction preserved after rainfall (Fig. 10) and also their higher mechanical pull-out resistances as compared to the other two geometries (Kamchoom et al. 2014). On the contrary, the slope supported by the plate-shaped roots is only marginally safe (i.e. FOS close to 1.0; Fig. 12). As no suction was preserved (Fig. 10c), the shallow slope stability was mainly contributed by the soil strength itself and the mechanical root reinforcement. As all plate-shaped roots have no taproot component, the pull-out resistance provided by this root geometry has only one third of that mobilised in the tap- and heart-shaped root (Kamchoom et al. 2014), thereby contributing relative less to the slope stability.

Figure 12 also shows the FOS of the three types of slopes that ignored the transpiration process before the rainfall event. It can be seen that the values of FOS after rainfall are all less than 1.0, indicating potential slope failure. The major reason is that when ignoring the effects of transpiration, no suction was preserved in all three slopes and a significant amount of positive PWP was developed hydrostatically along depth after the rainfall (see Fig. 10). Following such substantial increase in PWP, strain localisation occurred at relatively shallower region and closer to the toe of each slope (Fig. 13j–l). Regardless of the root geometry, neglecting the effects of transpiration on slope stability resulted in a significant drop of FOS by up to 50 %.

Summary and conclusions

This paper interprets a comprehensive set of centrifuge model test data. The effects of root geometries and transpiration-induced suction on slope stability were quantified and compared. Three types of new artificial roots with different representative geometries (i.e. tap, heart and plate) were designed to enable the effects of transpiration to be simulated in centrifuge. These roots possessed mechanical properties closely resembling those real roots found in the field. The observed behaviour of slope models supported by the three different types of artificial roots was back-analysed through a series of finite element seepage-stability analyses to enhance the understanding of slope stability against intense rainfall.

The centrifuge tests revealed that the root geometry has a strong effect on both the magnitude and distribution of transpiration-induced suction. The heart-shaped root created the highest suction of 30 kPa within the root depth because this

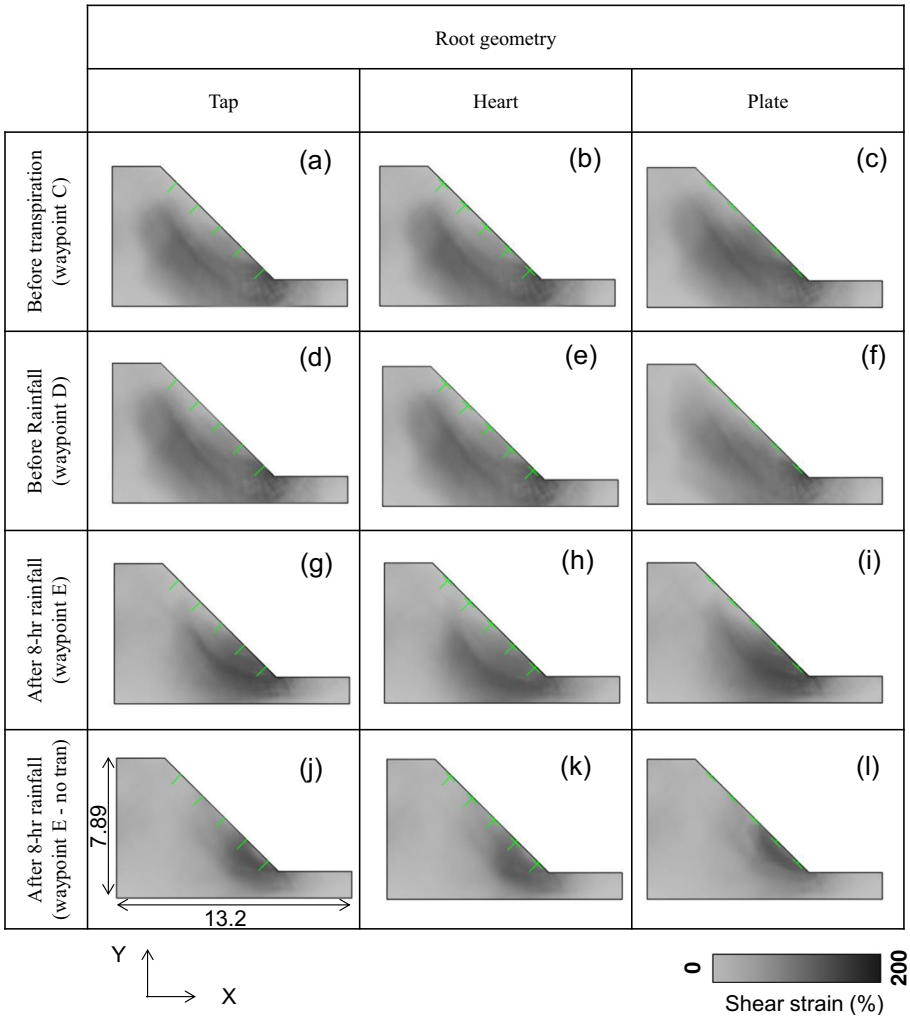

Fig. 13 Computed shear strain contours in slopes supported by tap-, heart- and plate-shaped roots before transpiration (**a**–**c**), before rainfall (**d**–**f**), after 8-h rainfall (**g**–**i**) and after 8-h rainfall without considering transpiration (**j**–**l**) (all dimensions are in meters and in prototype scale)

geometry has the highest soil-root contact area for water uptake among the three geometries tested. More importantly, the higher suction induced by the transpiration process consequently resulted in a lower water infiltration rate during the subsequent rainfall event. Following an extreme rainfall event with an equivalent return period of 1000 years, a uniform distribution of suctions was retained within the root depth in the tap-shaped root and heart-shaped root cases. Because of the relatively shallow depth of the plate-shaped roots (i.e. 0.1 m), all suctions developed in the previous drying period disappeared, and some positive PWPs were built-up.

The PWP responses measured in all three centrifuge tests were captured reasonably well by the transient seepage analyses, when the sets of drying and wetting soil hydraulic properties were used to model the processes of transpiration and rainfall, respectively. When both the hydrological and mechanical effects of roots were considered, the slope supported by the heart-shaped artificial roots provided the highest FOS after rainfall (16 and 28 % higher than that supported by the tap- and plated-shaped roots, respectively). It is revealed that for any types of root geometry, ignoring the shear strength contributed by the transpiration-induced suction would result in much lower values of FOS (i.e. more than 50 % lower than the case with transpiration simulation) and shallower maximum shear strain given the same rainfall event.

Acknowledgments

A research grant (HKUST6/CRF/12R) provided by the Research Grants Council of the Government of the Hong Kong SAR and another one (2012CB719805) provided by the Ministry of Science and Technology of the People's Republic of China under the National Basic Research Program (973 Program) are acknowledged. The third author would also like to acknowledge the funding provided by the EU FP7 Marie Curie Career Integration Grant (CIG) under the project "BioEPIC slope", as well as research travel support from the Northern Research Partnership (NRP).

References

Adhikari AR, Gautam MR, Yu Z, Imada S, Acharya K (2013) Estimation of root cohesion for desert shrub species in the Lower Colorado riparian ecosystem and its potential for streambank stabilization. Ecol Eng 51:33–44

Bischetti GB, Chiaradia EA, Simonato T, Speziali B, Vitali B, Vullo P, Zocco A (2005) Root strength and root area ratio of forest species in Lombardy, Northern Italy. Plant Soil 278(1–2):11–22
Bolton MD, Gui MW, Phillips R (1993) Review of miniature soil probes for model tests. In: Proceedings of the 11th Southeast Asian Geotechnical Conference, Hong Kong, pp 85–90
BSI (1990) Methods of test for soils for civil engineering purposes. Compaction-related tests. Standard BS 1377-4:1990. British Standards Institution (BSI), London
Caicedo B, Tristancho J (2010) A virtual rain simulator for droplet transport in a centrifuge. In: Proceedings of the 7th International Conference on Physical Modelling in Geotechnics (ICPMG 2010), Zurich, pp 99
Coppin NJ, Richards IG (1990) Use of vegetation in civil engineering. Butterworths, London
Coutts MP (1986) Components of tree stability in Sitka spruce on peaty gley soil. Forestry 59(2):173–197
Coutts MP, Nielsen CCN, Nicoll BC (1999) The development of symmetry, rigidity and anchorage in the structural root system of conifers. Plant Soil 217(1–2):1–15
Dawson EM, Roth WH, Drescher A (1999) Slope stability analysis by strength reduction. Geotechnique 49(6):835–840
De Baets S, Poesen J, Reubens B, Wemans K, De Baerdemaeker J, Muys B (2008) Root tensile strength and root distribution of typical Mediterranean plant species and their contribution to soil shear strength. Plant Soil 305(1–2):207–226
Dell'Avanzi E, Zornberg JG, Cabral A (2004) Suction profiles and scale factors for unsaturated flow under increased gravitational field. Soils Found 44(3):1–11
Docker BB, Hubble TCT (2008) Quantifying root-reinforcement of river bank soils by four Australian tree species. Geomorphology 100:401–418
Fan CC, Chen YW (2010) The effect of root architecture on the shearing resistance of root-permeated soils. Ecol Eng 36(6):813–826
Geo-Slope International Ltd. (2009) Seepage modeling with SEEP/W, an engineering methodology, 4th Edn
Geo-Slope International Ltd. (2009) Stress-deformation modeling with SIGMA/W, an engineering methodology, 4th Edn
Ghestem M, Veylon G, Bernard A, Vanel Q, Stokes A (2014) Influence of plant root system morphology and architectural traits on soil shear resistance. Plant Soil 377(2):43–61
Griffiths DV, Lane PA (1999) Slope stability analysis by finite elements. Geotechnique 49(3):387–403
Hau BC, Corlett RT (2003) Factors affecting the early survival and growth of native tree seedlings planted on a degraded hillside grassland in Hong Kong, China. Restor Ecol 4(11):483–488
Hinton E, Owen DRJ (1979) An introduction to finite element computations. Pineridge Press Ltd., UK
Ho MY (2007) Governing parameters for stress-dependent soil-water characteristics, conjunctive flow and slope stability. PhD Thesis, The Hong Kong University of Science and Technology
Hossain MA, Yin JH (2010) Shear strength and dilative characteristics of an unsaturated compacted completely decomposed granite soil. Can Geotech J 47(10):1112–1126
Indraratna B, Redana IW (1997) Plane-strain modeling of smear effects associated with vertical drains. J Geotech Geoenviron Eng ASCE 123(5):474–478
Kamchoom V, Leung AK, Ng CWW (2014) Effects of root geometry and transpiration on pull-out resistance. Geotechnique Lett 4(4):330–336. doi:10.1680/geolett.14.00086
Kim Y, Lee S, Jeong S, Kim J (2013) The effect of pressure-grouted soil nails on the stability of weathered soil slopes. Comput Geol 49:253–263
Köstler JN, Bruckner E, Bibelriether H (1968) Die Wurzeln der WaldbQume. Verlag Paul Parey, Hamburg
Ladd RS (1977) Specimen preparation and cyclic stability of sands. J Geotech Eng Div 6(103):535–547
Lam CC, Leung YK (1995) Extreme rainfall statistics and design rainstorm profiles at selected locations in Hong Kong. Royal Observatory, Hong Kong
Leung TY (2014) The use of native woody plants in slope upgrading in Hong Kong, PhD Thesis, The University of Hong Kong
Leung AK, Ng CWW (2013a) Seasonal movement and groundwater flow mechanism in an unsaturated saprolitic hillslope. Landslides 10(4):455–467
Leung AK, Ng CWW (2013b) Analysis of groundwater flow and plant evapotranspiration in a vegetated soil slope. Can Geotech J 50(12):1204–1218
Lim TT, Rahardjo H, Chang MF, Fredlund DG (1996) Effect of rainfall on matric suctions in a residual soil slope. Can Geotech J 33(4):618–628
McNamara AM, Taylor RN (2004) The influence of enhanced excavation base stiffness on prop loads and ground movements during basement construction. Struct Eng 82(4):30–36
Mickovski SB, Bengough AG, Bransby MF, Davies MCR, Hallett PD, Sonnenberg R (2007) Material stiffness, branching pattern and soil matric potential affect the pullout resistance of model root systems. Eur J Soil Sci 58(6):1471–1481
Ng CWW (2014) The state-of-the-art centrifuge modelling of geotechnical problems at HKUST. J Zhejiang Univ Sci A 15(1):1–21
Ng CWW, Leung AK (2012) Measurements of drying and wetting permeability functions using a new stress-controllable soil column. J Geotech Geoenviron Eng ASCE 138(1):58–68
Ng CWW, Pang YW (2000) Influence of stress state on soil-water characteristics and slope stability. J Geotech Geoenviron Eng ASCE 126(2):157–166
Ng CWW, Zhang LM, Ho KK (2001) Influence of laterally loaded sleeved piles and pile groups on slope stability. Can Geotech J 38(3):553–566
Ng CWW, Woon KX, Leung AK, Chu LM (2013) Experimental investigation of induced suction distributions in a grass-covered soil. Ecol Eng 52:219–223
Ng CWW, Leung AK, Kamchoom V, Garg A (2014) A novel root system for simulating transpiration-induced soil suction in centrifuge. Geotech Test J 37(5):1–15
Ovesen NK (1979) Discussion on "The use of physical models in design". In: Proceedings of 7th European Conference in Soil Mechanics, Brighton, 319–323
Perry TO (1989) Tree roots: facts and fallacies. Arnoldia 49(4):3–24
Powrie W (1986) The behaviour of diaphragm walls in clay. PhD thesis, University of Cambridge, U.K.
Simon A, Collison AJ (2002) Quantifying the mechanical and hydrologic effects of riparian vegetation on streambank stability. Earth Surf Process Landf 27(5):527–546
Sonnenberg R, Bransby MF, Hallett PD, Bengough AG, Mickovski SB, Davies MCR (2010) Centrifuge modelling of soil slopes reinforced with vegetation. Can Geotech J 47(12):1415–1430
Sonnenberg R, Bransby MF, Bengough AG, Hallett PD, Davies MCR (2012) Centrifuge modelling of soil slopes containing model plant roots. Can Geotech J 49(1):1–17
Stokes A, Mattheck C (1996) Variation of wood strength in tree roots. J Exp Bot 47(5):693–699
Stokes A, Ball J, Fitter AH, Brain P, Coutts MP (1996) An experimental investigation of the resistance of model root systems to uprooting. Ann Bot 78(4):415–421
Take WA, Bolton MD, Wong PCP, Yeung FJ (2004) Evaluation of landslide triggering mechanisms in model fill slopes. Landslides 1(3):173–184
Taylor RN (1995) Geotechnical centrifuge technology. Taylor and Francis
van Genuchten MT (1980) A closed-form equation for predicting the hydraulic conductivity of unsaturated soils. Soil Sci Am J 44(5):892–898
Vanapalli SK, Fredlund DG, Pufahl DE, Clifton AW (1996) Model for the prediction of shear strength with respect to soil suction. Can Geotech J 33(3):379–392
Wang LP, Zhang G (2014) Centrifuge model test study on pile reinforcement behavior of cohesive soil slopes under earthquake conditions. Landslides 11(2):213–223
Wang CL, Liu J, Xing HW, Yao XJ, Wang LH, Niu GQ (2010) Friction properties of interface between soil-roots and soil-soil of Artemisia sphaerocephala and Sabina valgaris. In: Proceedings of 4th International Conference on Bioinformatics and Biomedical Engineering, Chengdu, pp 1–5
Yang MZ, Drumm EC (2000) Numerical analysis of the load transfer and deformation in a soil nailed slope. Numerical Methods in Geotechnical Engineering, ASCE, 102–116
Zhou ZB (2008) Centrifuge and three-dimensional numerical modelling of steep CDG slopes reinforced with different sizes of nail heads. PhD Thesis, The Hong Kong University of Science and Technology

C. W. W. Ng · V. Kamchoom (✉)
Department of Civil and Environmental Engineering,
Hong Kong University of Science and Technology,
Hong Kong, Hong Kong
e-mail: kviroon@ust.hk

A. K. Leung
School of Science and Engineering,
University of Dundee,
Fulton Building, Dundee, UK